

Selected Paper

Electrochemical Oxidation Properties of Tetrakis(*tert*-butyl)-phthalocyaninatozinc(II) in Non-Aqueous Media: A Reinvestigation into the Effects of Stacking, Axial Coordination, and Solvent

Mitsuhiko Morisue,*,† Kazuya Kameyama, and Yoshiaki Kobuke*,††

Graduate School of Materials Science, Nara Institute of Science and Technology, Ikoma 630-0192

Received December 16, 2008; E-mail: morisue@kit.ac.jp

The electrochemical oxidation properties of tetrakis(*tert*-butyl)phthalocyaninatozinc, Zn(*t*-Bu_4Pc), has been reinvestigated for the first systematic exploration in comparison with the authentic properties of porphyrin. The experimental conditions for the oxidation properties of the monomeric Zn(*t*-Bu_4Pc) species were optimized in CH_2Cl_2 as a non-coordinating solvent to exclude the effect of axial coordination, although most of the previous studies employed coordinating solvents to overcome poor solubility. Employing dilute conditions with 0.1 M tetra-*n*-butylammonium hexafluorophosphate (*n*-$Bu_4N\cdot PF_6$) as a supporting electrolyte, the effect of axial ligand and solvent on the oxidation behaviors of Zn(*t*-Bu_4Pc) were newly analyzed. The effects of axial coordination on the oxidation properties of Zn(*t*-Bu_4Pc) are discussed from the views of the kinetic process in the charge-compensating step, the structural deformation by axial coordination, and the σ-donation from the axial ligand to the d-orbital of the central zinc. Coordination of axial ligand and polar solvent results in an unusual positive shift of the oxidation potential of Zn(*t*-Bu_4Pc). We propose a ligand dissociation mechanism for the oxidation processes of Zn(*t*-Bu_4Pc) as a rational explanation for the experimental observations. The relevance of the electrochemical properties is supported by spectroscopic characterization.

Metallophthalocyanines, M(Pc)s, have served widely as practical dyes and pigments for extensive applications, such as electrical conductors, charge carriers in photocopies, optical memory, photosensitizers, and inks, based on high thermal and chemical stability with large molar extinction coefficient of Q-bands in the near-IR region and excellent redox properties.[1] Furthermore, recent progress of tailored Pc systems is about to emerge as novel functional molecular materials.[2] Redox properties of M(Pc)s are essential for prediction of electron-transfer reactions and electronic structures in developing photoelectronic devices. Besides, insight into the electrochemistry of M(Pc)s will help understanding biological electron-transfer systems, because 18π porphyrinoids are fundamental chromophores of photosynthetic pigments and heme proteins. According to Marcus' prediction,[3] interplays between the redox sites and surrounding peptide scaffold play crucial roles in determining the efficiency of biological electron transfer. Thus, the effect of surrounding media on the electrochemical properties of M(Pc)s is important for understanding basic chemistry in electron-transfer reactions from the view of both material and biological sciences. The redox-inert zinc(II) center allows us to evaluate the redox properties of macrocyclic Pc ligand. The present paper is aimed at elucidating the fundamental electrochemical oxidation properties of Zn(Pc).

The electrochemical properties of Zn(Pc) molecules have been characterized in a number of studies.[1] To obtain well-resolved voltammograms, the electrochemical investigation has been undertaken in coordinating solvents[1,4,5] or under unusual conditions.[6] Otherwise, well-resolved voltammogram require bulky peripheral substituents.[7] Some reports ignored aggregation in *o*-dichlorobenzene.[8] Based on a survey of this previous research, poor solubility of Zn(Pc) seems to have hampered formation of monomeric Zn(Pc) in non-coordinating solvent. These reports have neglected the effect of axial coordination, but there is no elucidation whether such effect is really negligible. For metalloporphyrins, on the other hand, the effect of axial ligands and electrolytes on the redox couples has been established well through studies by Kadish et al. and other groups.[9–13] These effects on the redox properties of Zn(Pc)s have not been explored so far, despite the importance. Hence, we have herein reinvestigated the electrochemical properties of Zn(Pc) mainly in dichloromethane as a non-coordinating solvent.

The oxidation potential of tetrakis(*tert*-butyl)phthalocyaninatozinc(II), Zn(*t*-Bu_4Pc) (Scheme 1), is herein exploited in common non-aqueous solvents. Even though Zn(*t*-Bu_4Pc) bears bulky peripheral substituents, the first oxidation wave of Zn(*t*-Bu_4Pc) is still split by aggregation. Optimization of the experimental conditions, such as dilute concentration in the presence of appropriate supporting electrolyte, avoids the

† Present address: Department of Biomolecular Engineering, Kyoto Institute of Technology, Matsugasaki, Sakyo-ku, Kyoto 606-8585

†† Present address: Institute of Advanced Energy, Kyoto University, Gokasho, Uji, Kyoto 611-0011

Published on the web May 13, 2009; doi:10.1246/bcsj.82.574

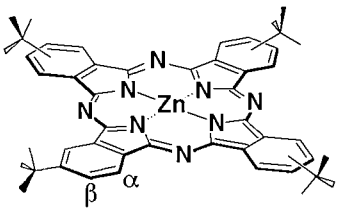

Scheme 1. Chemical structure of Zn(*t*-Bu_4Pc).

aggregation and ensures observation of the intrinsic redox properties of monomeric Zn(*t*-Bu_4Pc). Based on the systematic experiments, the effects of axial coordination of nitrogenous ligand, counter ion, and solvent on the oxidation potentials will be elucidated.

Results and Discussion

Effect of Stacking/Disstacking. In the case of porphyrin, CH_2Cl_2 is generally used as solvent for electrochemical measurements, because of a distinct advantage in comparing photophysical measurements and chemical reactions with those in non-coordinating solvents.[14] Zn(*t*-Bu_4Pc) still tends to aggregate in less polar solvents even though bulky peripheral *tert*-butyl groups are attached. The experimental conditions for Zn(*t*-Bu_4Pc) were therefore optimized in CH_2Cl_2. At 1.0 mM of Zn(*t*-Bu_4Pc), Zn(*t*-Bu_4Pc) shows multistep oxidation waves due to aggregation (Figure 1c). On dilution up to 0.1 mM, the first oxidation waves converged to a single redox couple around 447 mV vs. Ag/AgCl (Figure 1a). The single oxidation wave around 447 mV is therefore assignable to the first ring oxidation of monomeric Zn(*t*-Bu_4Pc). This assignment is consistent with the monomeric spectral shape in UV–vis absorption spectrum (as shown in Figure 3, vide infra).

Zn(*t*-Bu_4Pc) aggregation appeared to make a remarkable positive shift of the first oxidation potential in CH_2Cl_2. When one considers the association behavior during redox processes, aggregation of the neutral species and association of cationic species with the neutral must be different from each other. It is known that oxidized aromatic species often attract neutral species via cation–π interaction. For example, the monomeric Co(Pc) is reported to be observed in sufficiently fast potential sweep prior to dynamic aggregation by cation–π interaction.[13] On the other hand, the magnitude of the first oxidation wave of the monomeric Zn(*t*-Bu_4Pc) around 447 mV vs. Ag/AgCl proportionally increased as a function of the square root of the scan rate up to 200 mV s^{-1} (Figure 1d). At 0.5 mM, an additional peak accompanied around 600 mV and both peaks increased as a function of the root of sweep rate with quasi reversibility (Figure 1e). Oxidation processes of Zn(*t*-Bu_4Pc) aggregates are thus governed by electron-transfer kinetics, suggesting that the dynamic aggregation by cation–π interaction is negligible. Static aggregation occurred dominantly in the neutral state without dynamic aggregation in the CV time scale.

Potential shift from 447 to 600 mV for the first oxidation in stacked Zn(*t*-Bu_4Pc) may arise from intervalence (charge-resonance) interaction of cofacially stacked Pc rings. In our previous study, the cofacially coordinated Zn(Pc) dimer showed split oxidation waves, where the first oxidation potential was identical with that of the corresponding monomer and the second one appeared at a more positive potential

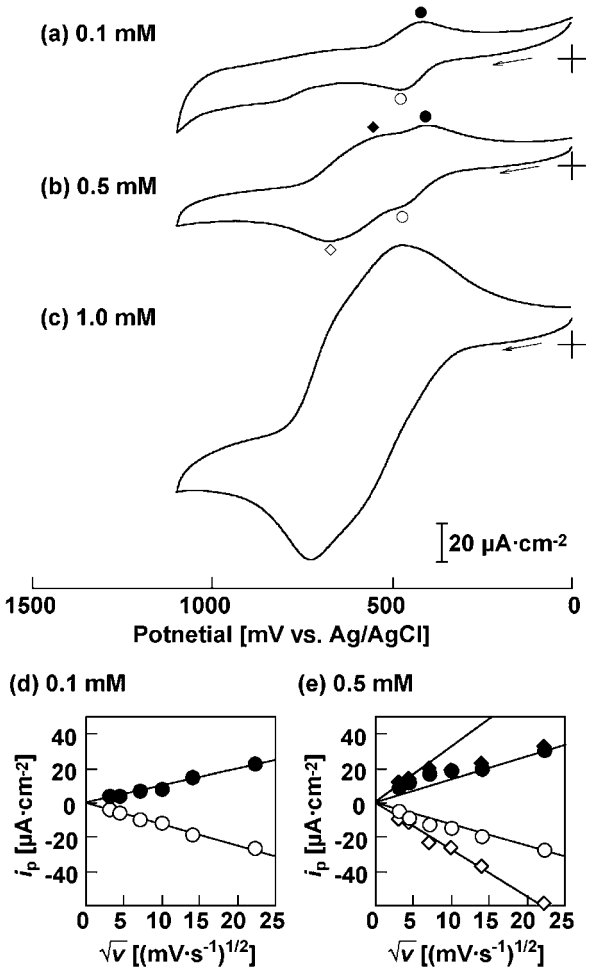

Figure 1. Cyclic voltammograms at various concentrations of Zn(*t*-Bu_4Pc) with 0.1 M *n*-$Bu_4N \cdot PF_6$ as a supporting electrolyte in CH_2Cl_2 at 25 °C with a scan rate of 50 mV s^{-1}: (a) 0.1, (b) 0.5, and (c) 1.0 mM of Zn(*t*-Bu_4Pc). The plot of the magnitude of peak current, i_p, as a function of square root of scan rate, $v^{1/2}$ (d and e), wherein open/closed circles/squares in the plots denote the corresponding peaks in CVs (a and b).

region.[15] Similar oxidation behavior was reported for the covalently bridged Zn(Pc) dimers.[16] Resemblance in the voltammograms of Zn(*t*-Bu_4Pc) aggregates suggests that the split oxidation waves are ascribable to the intervalence interaction through stacked Pc rings.[17] Due to the heterogeneity of size in Zn(*t*-Bu_4Pc) aggregates, the diversity of the intervalence states provided manifold redox potentials at 1.0 mM (Figure 1c). Such intervalence properties are relevant to metallic conductivity in vacuum-deposited films.[18]

Zn(Pc)s are reported to aggregate themselves with association constants in the order of 10^4 M^{-1} in benzene or dodecane.[19] Judging from the concentration dependence in CVs (Figures 1a–1c), the present observation for Zn(*t*-Bu_4Pc) in CH_2Cl_2 is consistent with these reports. The electrochemical measurement at 0.1 mM Zn(*t*-Bu_4Pc) may show a single peak without aggregation during CV potential sweep cycles. The following experiments were therefore carried out at a concentration of 0.1 mM of Zn(*t*-Bu_4Pc).

Effect of Supporting Electrolyte. Electrochemical oxidation steps postulate charge compensation with the counter anion from the supporting electrolyte. Thus, the supporting electrolyte affects sensitively the oxidation potential. For instance, Lever and Wilshire reported that the oxidaton potential of the central $Fe^{III/II}$ of Fe(Pc) coupled with anion binding.[20] In oxidation steps of zinc porphyrin, solvent molecule on the central metal is displaced by counter anion, and therefore the oxidation potentials are affected despite the closed shell nature of the central zinc(II) ion.[10–12] Herein, *n*-$Bu_4N\cdot PF_6^-$ was compared with *n*-$Bu_4N\cdot ClO_4$.

In the presence of *n*-$Bu_4N\cdot PF_6$, Zn(*t*-Bu_4Pc) was oxidized at 447 mV vs. Ag/AgCl (−13 mV vs. Fc^+/Fc). This oxidation potential is much more negative than that of 610 mV vs. Ag/AgCl (155 mV vs. Fc^+/Fc) with *n*-$Bu_4N\cdot ClO_4$. Although the electrolyte is assumed not to interact with neutral Zn(*t*-Bu_4Pc), the anion may have affected the oxidation potentials of $Zn(t\text{-}Bu_4Pc)^{+/0}$ by ion-pair formation with the π-cation radical, $Zn(t\text{-}Bu_4Pc)^{+\bullet}$, during the electrochemical oxidation processes. The process in CH_2Cl_2 containing 0.1 M *n*-$Bu_4N\cdot X$ as the supporting electrolyte, is expressed as follows;[10,11]

$$Zn(t\text{-}Bu_4Pc) + X^- \rightarrow Zn(t\text{-}Bu_4Pc)^{+\bullet}\cdot X^- + e^- \quad (1)$$

The ion-pairing affinity to π-cation radical $Zn(t\text{-}Bu_4Pc)^{+\bullet}$ may be stronger for PF_6^- than ClO_4^-. Weakly binding ClO_4 anion afforded un-resolved waves in the voltammograms, probably due to poor solubility of non-coordinated species and/or aggregation. It is reported that the cation radical of zinc porphyrin interacts more strongly with ClO_4^- than PF_6^-.[10–12] The effect of the counter anion on half-wave potential could be attributed to the difference in the activation energy for association/dissociation of cation radical and the counter anion. At this moment, it is difficult to determine the dominant factor of the supporting electrolyte. Further extensive experiments are required to elucidate such effect of the counter anion on the oxidation potential shift of Zn(*t*-Bu_4Pc). The present paper describes below the effects of axial ligand and solvent by employing *n*-$Bu_4N\cdot PF_6$ as a supporting electrolyte.

Effect of Axial Coordination. Axial coordination induced large positive shift of the oxidation potential of Pc macrocycle. Addition of pyridine as an axial ligand to Zn(*t*-Bu_4Pc) in CH_2Cl_2 lead to splitting of the first oxidation wave around 447 mV into two waves (Figure 2b). Further addition of pyridine resulted in the appearance of the third oxidation wave (triangles in Figure 2) around 760 mV with disappearance of the oxidation wave of ligand-free species (circles in Figure 2). Therefore, addition of pyridine leads to the appearance of two characteristic oxidation waves. This fact requires at least two factors influencing the oxidation properties of Pc macrocycles. We will discuss below a possible mechanism.

Competitive Binding Mechanism: The positive shift of the oxidation potentials of Zn(*t*-Bu_4Pc) by the presence of pyridine may be interpreted as the contribution of competitive binding of the axial ligand with supporting electrolyte, in a manner similar to the zinc porphyrin system.[9] The competitive binding process is given as eq 2.

$$Zn(t\text{-}Bu_4Pc)\cdot L + X^- \rightarrow Zn(t\text{-}Bu_4Pc)^{+\bullet}\cdot X^- + L + e^- \quad (2)$$

When the ligand strongly coordinates to cation radical

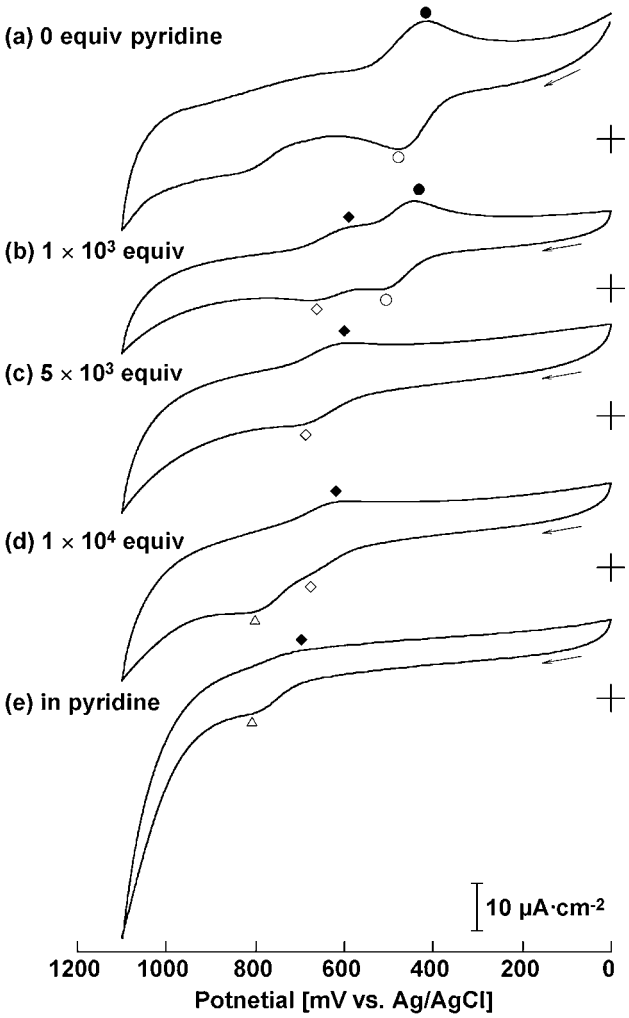

Figure 2. Cyclic voltammograms of 0.1 mM Zn(*t*-Bu_4Pc) with 0.1 M *n*-$Bu_4N\cdot PF_6$ as a supporting electrolyte in the presence of various amounts of pyridine in CH_2Cl_2: (a) with 0 mM of pyridine (same with Figure 1a), (b) with 100 mM of pyridine, (c) with 500 mM of pyridine, (d) with 1.0 M of pyridine, and (e) in neat pyridine. The voltammograms were observed at a sweep rate of 50 mV s^{-1} at 25 °C. Under these conditions, the oxidation of ferrocene internal standard ($Fc^{+/0}$) was observed at 460 mV vs. Ag/AgCl except for in neat pyridine at 546 mV.

$Zn(t\text{-}Bu_4Pc)^{+\bullet}$, replacement of the ligand by anion should be suppressed. Competition of charge compensation with the axial ligand requires higher potential application. Another process to be considered is electrostatic ion-pair formation with axially coordinating species as eq 3.

$$Zn(t\text{-}Bu_4Pc)\cdot L + X^- \rightarrow [Zn(t\text{-}Bu_4Pc)\cdot L]^{+\bullet}\cdot X^- + e^- \quad (3)$$

Addition of axial ligand reduced amplitudes of the oxidation waves. Namely, the axial ligand diminished the diffusion coefficient. The diffusion coefficient (D_0) is defined by the Stokes–Einstein equation as a function of the Stokes radius (r_s) ($D_0 = RT/6\pi\eta r_s N_A$, wherein R is the gas constant, T is absolute temperature, η is dynamic viscosity of the solvent, and N_A is Avogadro's number).[21] The axially bound ligand apparently increased the Stokes radius of the redox site. The

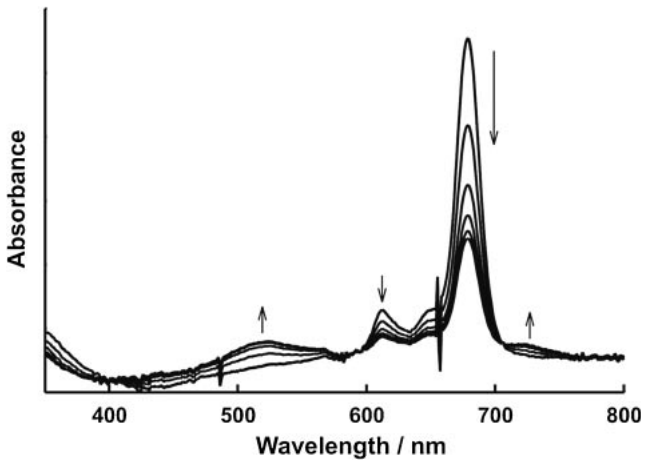

Figure 3. Spectral change of 0.1 mM Zn(*t*-Bu_4Pc) with 0.1 M *n*-$Bu_4N \cdot PF_6$ in CH_2Cl_2 from 0 to 30 s under electrolysis at a potential of 1.9 V vs. Ag wire.

competitive binding mechanism is one possible explanation for the potential shift.

Spectral Change during Electrolysis: Spectroscopic characterization of the radical species will give distinct information on the electrochemical species. We measured the cation radical in CH_2Cl_2 to clarify the difference between Zn(*t*-Bu_4Pc)$^{+\bullet} \cdot PF_6^-$ and [Zn(*t*-Bu_4Pc)$\cdot$L]$^{+\bullet} \cdot PF_6^-$ under aerobic conditions. Exhaustive electrolysis at a potential of 1.9 V vs. Ag wire (corresponding to ≈0.7 V vs. Ag/AgCl) led to gradually decreasing Q-band and new bands appeared around 520 and 725 nm through isosbestic points in CH_2Cl_2 (Figure 3). The spectrum was similar to that obtained in the case of [Zn(Pc)$\cdot$Im]$^{+\bullet} \cdot ClO_4^-$.[5b] This coincidence suggests that the axial ligand is dissociated from the cation radical (eqs 2 and 3). This assumption is consistent with the fact that the third oxidation wave (triangle in Figure 2) is accompanied by no corresponding new reduction peak. Such irreversibility of the oxidation in pyridine will be attributed to replacement of the axial ligand by the counter electrolyte.

Structural Relaxation: The electrochemical kinetics must determine primarily the redox process, but it is not directly correlated with the intrinsic properties of HOMO and LUMO levels. If the positive shift observed is ascribed to the step generating [Zn(*t*-Bu_4Pc)$\cdot$L]$^{+\bullet} \cdot PF_6^-$ (eq 3), electronic parameters other than the electrochemical kinetics may be required for interpreting the redox properties of Zn(Pc). The structural view may account for the positive shift of the oxidation potential. Recently, Kobayashi et al. elucidated that the distortion of Pc macrocycle by steric conflict of the bulky phenyl groups at α-positions (non-square-pyramidal conformation) leads to a negative shift of the oxidation potential and a bathochromic shift of the absorption band.[22] However, in the titration experiment of Zn(*t*-Bu_4Pc) by addition of axial ligand, only a marginal spectral change is observed.[15] X-ray crystallographic data shows that tetra-coordinated neutral species of Zn(Pc) is in a planar conformation with D_{4h} geometry, thereby the Pc macrocycle is expanded because the radius of the central zinc(II) is too large to be accommodated in the tetrapyrrolic cavity of the Pc ligand.[23] In contrast to Kobayashi's sterically

Table 1. Effect of Axial Ligand (1.0×10^4 equiv) on Half-Wave Potentials of 0.1 mM Zn(*t*-Bu_4Pc) with 0.1 M *n*-$BuN_4 \cdot PF_6$ in CH_2Cl_2[a)]

Axial ligand	Zn(*t*-Bu_4Pc)$^{+/0}$ (ΔE_p) [mV vs. Ag/AgCl]
—	447 (60)
Pyridine (Py)	613 (85)
3-Acetylpyridine (PyAc)	652 (86)
3-Chloropyridine (PyCl)	657 (61)
3-Cyanopyridine (PyCN)	663 (93)
1-Methylimidazole (MeIm)	557 (98)

a) ΔE_p: Potential peak separation at a scan rate of 50 mV s^{-1}. Under these conditions, the oxidation of ferrocene internal standard ($Fc^{+/0}$) was observed at 460 mV vs. Ag/AgCl.

strained Pc, axial coordination dislocates the central zinc by 0.48 Å from the Pc N_4-plane, so that the planar Pc macrocycle is distorted to a square-pyramidal conformation.[24] Such a large structural change occurs by the unusually short N–Zn distance of Zn(Pc).[23] Large dislocation of zinc atom releases the structural strain of neutral Zn(Pc) to elongate the N–Zn distance from 1.98 to 2.06 Å, with a small distortion of Pc macrocycle in the X-ray crystallography.[24] This mechanism will be most probably pertinent to the extremely large potential shift. In the present experiment, addition of pyridine resulted in larger positive shifts than the case of 1-methylimidazole, despite decreased coordination ability (see Table 1, vide infra). This discrepancy may be ascribable to the difference of steric hindrance of the proton α to nitrogen atom of the axial ligand to dislocate the central zinc out of the Pc N_4-plane.[25] Therefore positional change of zinc atom by axial coordination is likely to account for the large potential shift of the oxidation potentials, even though other factors may also be conceivable.

Plausible Mechanism: Based on the above considerations, we propose a tentative mechanism for the behavior of oxidation potentials (Scheme 2). When no ligand coordinates to the central zinc, counter anion is readily accessible for charge-compensation (eq 1). Upon addition of pyridine, the initial splitting of the oxidation wave (Figure 2b) is attributed to competitive anion binding to replace the axial ligand (eq 2). Splittings of oxidation waves suggest that the axial coordination follows very slow kinetics in the CV sweep time range.

Further addition of pyridine leads to the third oxidation wave (triangle in Figures 2d and 2e). The third oxidation wave will be assignable to the electrostatic complexation with the axial ligand bound cation radial, [Zn(*t*-Bu_4Pc)$\cdot$L]$^{+\bullet} \cdot X^-$ (eq 3). After electrostatic complexation, the axial ligand on cation radical is replaced by the counter anion to provide Zn(*t*-Bu_4Pc)$^{+\bullet} \cdot X^-$. The last process should be electrochemically silent. This interpretation is in line with the fact that the third oxidation is not accompanied by a corresponding new reduction wave instead of the ligand-competitive wave (filled-squares in Figures 2d and 2e). Thus, the influence of competing counter anion (eq 2) cannot be avoided for the whole oxidation processes, whereby the intrinsic potentials may be more positive than the observed half-wave potentials. This mechanism may be most compatible with the present observations at this moment, although not definitive. Alternatively, the

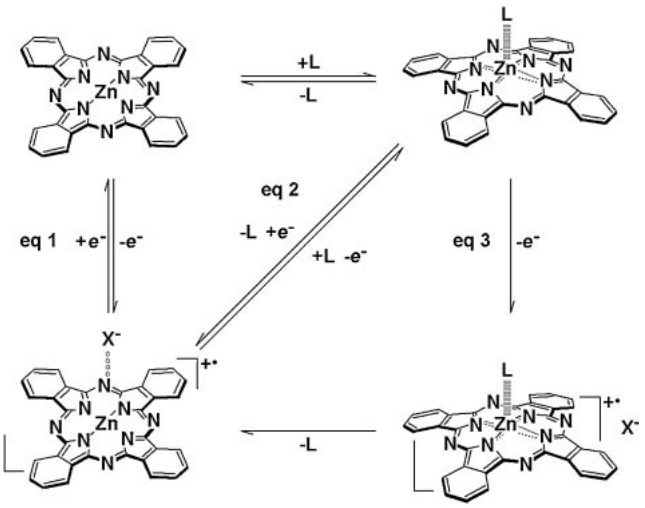

Scheme 2. Plausible mechanism of oxidation of Zn(Pc) with axial ligand (L). *t*-Butyl groups are omitted for visual clarity.

oxidation processes may be governed by at least two dominant factors, such as kinetic and structural parameters.

Charge Density of Central Zinc: As a last possible factor, the charge density of central zinc is described. Axial coordination of σ-donor increases the charge density of the central metal by interaction of the e_g–π orbital with metal d-orbital.[26] Lever and Minor elucidated that redox properties for redox-inactive metal-centered Pcs by changing the polarizing power of the central metal ion in DMF.[4] Both the first oxidation and reduction potentials of M(Pc)s shift linearly as a function of the charge density of the central metal.[4] Based on this observation, we attempted to tune the oxidation potential by σ-donation of axial ligand. Opposite to Lever's report, our experiments showed positive shift by the addition of axial ligand for all cases. A factor interfering with the effect of axial ligand may account for these unexpected observations in oxidation process. Hence, the results in the present trial are compatible with both the proposed mechanism and the Lever report, since dissociation of the axial ligand from the cation radical cannot ensure its influence on the oxidation potential. For instance, the electron-withdrawing group on pyridine did not lead substantial shift of the half-wave potential (Table 1). Furthermore, 1-methylimidazole (MeIm), a strongly coordinating ligand to neutral Zn(*t*-Bu_4Pc), showed smaller effect on the oxidation potential compared to the cases of pyridines. These trends imply that the positional movement of central zinc atom by axial coordination is significant rather than the σ-donation from the axial ligand, even if the effect of the axial coordination is limited only in the neutral Zn(Pc). Although the ligand dissociation process may disturb observing the effect of axial ligand, the oxidation process in eq 3 should reflect the intrinsic oxidation potential of $[Zn(Pc)\cdot L]^{+\bullet}$. Consequently, the preferential stabilization of the neutral species may be predominant in positive shift by addition of the axial ligand.

Solvent Dependence of Oxidation Potentials of Zn(*t*-Bu_4Pc). Electrochemical studies of M(Pc)s have been reported to shift to positive potentials on increasing the solvent polarity.[1] However, there has yet been no thorough and accurate exploration of Zn(Pc). Conventionally, electrochemical experiments for Pc's have employed coordinating solvent, e.g., DMA,[5] DMSO,[5c] DMF,[4,5c] and pyridine[27] to overcome the poor solubility. For measurements in non-coordinating solvents, axial ligands are sometimes required. Herein we examined the first systematic solvent effect on the electrochemical properties of Zn(Pc) under conditions excluding aggregation (0.1 mM of Zn(*t*-Bu_4Pc) with 0.1 M *n*-$Bu_4N\cdot PF_6$).

Table 2. Solvent Dependence of Half-Wave Potentials of Zn(*t*-Bu_4Pc) with 0.1 M *n*-$Bu_4N\cdot PF_6$

Solvent	DN/AN[a)]	$Fc^{+/0}$ [mV vs. Ag/AgCl]	Zn(*t*-Bu_4Pc)$^{+/0}$ (ΔE_p[b)]) [mV vs. Ag/AgCl]
CH_2Cl_2	0.0/20.4	460	447 (60)
PhCN	11.9/15.5	498	638 (74)
MeCN	14.1/18.9	426	437 (65)[c)]
THF	20.0/8.0	617	795 (66)
DMF	26.6/16.0	518	694 (120)
DMA	27.8/13.6	542	815 (53)
Py	33.1/14.2	546	760 (53)

a) DN/AN: donor/acceptor number. b) ΔE_p: Potential peak separation at 50 mV s^{-1}. c) Accompanying small additional wave ascribable to aggregated species.

Table 2 summarizes the solvent dependence of the half-wave potentials. The coordinating solvents enlarged the energy levels between neutral and π-cation radical of Zn(*t*-Bu_4Pc), so that the oxidation potential shifted toward positive potentials. The first oxidation Zn(*t*-Bu_4Pc)$^{+/0}$ showed a surprisingly large positive shift, from 447 mV in CH_2Cl_2 to 815 mV vs. Ag/AgCl in DMA. A similar positive shift of oxidation potential of Zn(*t*-Bu_4Pc) was observed in pyridine compared to that in CH_2Cl_2.[27] Even when the deviation by the liquid junction was excluded by using ferrocene as the standard reagent, the potential difference reached ca. 300 mV.

In general, the solvent effect on the shift of redox potential can be empirically discussed in correlation with the Gutmann donor number (DN), which is defined as the enthalpy for the coordination of donor solvent to $SbCl_5$ as the standard acceptor ($-\Delta H°(SbCl_5)$).[28] In the present case, the solvent effect on the half-wave potentials of Zn(*t*-Bu_4Pc) did not show clear correlation with the DN index (Figure S3).[29,30] The contribution of $[Zn(t\text{-}Bu_4Pc)\cdot L]^{+\bullet}\cdot PF_6^-$ may disturb the DN parameterization which describes the stability of a simple ion pair of Zn(*t*-Bu_4Pc)$^{+\bullet}\cdot PF_6^-$. The observed trends imply that polar solvents destabilize Zn(*t*-Bu_4Pc)$^{+\bullet}$ relative to neutral Zn(*t*-Bu_4Pc). This is opposite to the normal trend in redox processes, since the electrostatic complex should be stabilized in polar solvent. Based on the above considerations to the effect of axial ligand however, the oxidation process in the coordinating solvents may involve ligand dissociation. Briefly, the oxidation step of the neutral species is described as eq 3, while the reduction step of the cation radical is described as eq 2. Then the oxidation wave may include the intrinsic effect of solvent. Ligand dissociation interferes with the effect of axial coordination on the cation radical Zn(*t*-Bu_4Pc)$^{+\bullet}$, whereas the effect of axial ligand on the neutral species Zn(*t*-Bu_4Pc) remains. This assumption accounts for the preferential stabilization of Zn(*t*-Bu_4Pc) compared to Zn(*t*-Bu_4Pc)$^{+\bullet}$ in the

Table 3. Solvent Dependence of Absorption and Fluorescence Maximum of Zn(*t*-Bu$_4$Pc)

Solvent	n_D[a)]	ε_r[b)]	λ_{max}[c)]/nm (fwhm[e)]/cm^{-1})	λ_{em}[d)]/nm (fwhm/cm^{-1})	Φ_F[f)]
Toluene	1.45	2.4	677 (31)	679 (40)	0.23
CH_2Cl_2	1.42	8.93	678 (44)	681 (48)	0.25
PhCN	1.53	25.2	680 (44)	683 (45)	0.27
MeCN	1.34	35.9	673 (46)	675 (48)	0.25
THF	1.41	7.6	671 (42)	674 (44)	0.27
DMF	1.43	36.7	674 (44)	678 (48)	0.25
DMA	1.44	37.8	675 (42)	677 (45)	0.25
Py	1.51	12.9	680 (44)	684 (49)	0.27

a) n_D: refractive index. b) ε_r: dielectric constant. c) λ_{max}: absorption maximum. d) λ_{em}: emission maximum. e) fwhm: full width at the half maximum. f) Fluorescence quantum yield (Φ_F) was determined by $\lambda_{ex} = 612$ nm, based on the authentic value in toluene.[32]

apparent oxidation potential (half-wave potential) and large deviation from the linear correlation with the DN index.

Relevance to Spectroscopic Characterization. The oxidation potential must be related to the HOMO level. The HOMO and LUMO levels of Zn(*t*-Bu$_4$Pc) in various solvents are then evaluated by spectroscopic observation. Spectral properties observing the neutral state can exclude the complicated kinetic factors as observed in the electrochemical (ligand dissociation) process. Some M(Pc)s, wherein M = H_2, Co, Sn, and Sb, show solvatochromic shift of Q-band as a function of refractive index of the solvent (n_D).[31] In the case of Zn(*t*-Bu$_4$Pc), no solvatochromic effect on Zn(*t*-Bu$_4$Pc) was observed, HOMO (a_{1U})–LUMO (e_g) energy gap maintaining ca. 1.8 eV in any solvent (Table 3 and Figure S2). The Stokes shift of Zn(*t*-Bu$_4$Pc) ranged from 2 to 4 nm (corresponding to 4–11 cm^{-1}) with almost the same level (23–27%) of fluorescence quantum yield (Φ_F) in all the solvents. In general, the Stokes shift should change depending on the solvent polarity as defined by Mataga–Lippert equation.[33] According to this principle, the solvent-persistent Stokes shift requires that the solvent polarity strongly affects the electronic structure of Zn(*t*-Bu$_4$Pc) at the excited state (LUMO level). At the same time, marginal solvatochromism may imply that the HOMO level of Zn(*t*-Bu$_4$Pc) is perturbed similarly to the LUMO level by the solvent polarity to keep the energy gap almost constant. This is consistent with the fact that the absorption spectra showed only small change on titrating Zn(*t*-Bu$_4$Pc) with MeIm.[15] No substantial spectral change in the Q-band indicates that the HOMO–LUMO gap of the Pc macrocycle remains insensitive to axial coordination and also solvent variation. Combining the spectroscopic properties, the electronic structure of HOMO and also LUMO levels varies on solvent and/or axial ligand coordination. Therefore, the spectroscopic characterization is consistent with large potential shift observed in the electrochemical measurements, even though the positive potential shifts in the half-wave potentials are still underestimated because of ligand dissociation. Spectroscopic characterization in the static state supports the above consideration based on the electrochemical observation, that is structural relaxation of short N–Zn distance by axial coordination leading to the preferential stabilization of Zn(*t*-Bu$_4$Pc) compared to Zn(*t*-Bu$_4$Pc)$^{+\bullet}$ in addition to the kinetic parameter (ligand dissociation in the charge compensating process).

Conclusion

The intrinsic oxidation properties of Zn(*t*-Bu$_4$Pc) were investigated. It was elucidated that oxidation processes of Zn(*t*-Bu$_4$Pc) were influenced by stacking, solvent, and axial ligand, even though the absorption and emission spectra were not so sensitive to these effects. The present observation employed relatively dilute conditions with the consideration of strict experimental set-up and purity of the solvent and supporting electrolyte. Another optimization to observe monomeric species was required to determine accurately the reduction potentials of Zn(*t*-Bu$_4$Pc) in non-coordinating solvent to exclude non-Faradaic current in the reduction processes. We should give careful treatment to the experimental conditions and the redox potentials observed. Especially, solvent effects result in 300 mV of potential shift. Coordination of the axial ligand to the neural Zn(*t*-Bu$_4$Pc) while dissociation from cation radical Zn(*t*-Bu$_4$Pc)$^{+\bullet}$ by the charge-compensating anion may result in an unexpected shift of apparent oxidation potential observed. Such dynamic ligand dissociation accounts for the unusual solvent effect. The proposed mechanism is compatible with the spectroscopic properties. We should note the possibility that the apparent redox potential (half-wave potential) involves deviation from the intrinsic potential of Zn(*t*-Bu$_4$Pc) because of ligand dissociation–association in the redox process in polar solvent. At the same time, the oxidation wave should reflect the intrinsic redox potential, even if ligand dissociation occurs. These phenomena observed for the oxidation properties of Zn(*t*-Bu$_4$Pc) are important in relation to biological electron transfer. Actually, biological systems attenuate the redox potentials of porphyrin-related macrocycles embedded in protein scaffolds by controlling the environment and axial coordination.[3,34] Versatile electronic properties of Pc rings can meet wide-spread requirements for electronic and photonic materials. To modulate the electronic structure of Pc rings, several chemical modifications on the peripheral α- or β-positions of Zn(Pc)s have been systematically studied by Kobayashi et al.[35] The unique intrinsic feature of the oxidation properties of Zn(*t*-Bu$_4$Pc) will provide alternative and attractive opportunities to tune the redox potential of Pc macrocycle by aggregation, axial coordination, or environmental medium.[36]

Experimental

Materials and Abbreviations. Zn(*t*-Bu$_4$Pc) was prepared by one-pot cyclotetramerization from 4-*tert*-butyldiiminoisoindoline in the presence of zinc acetate in *N*,*N*-dimethylaminoethanol. 2,9(10),16(17),23(24)-Tetrakis(*tert*-butyl)phthalocyaninatozinc, Zn(*t*-Bu$_4$Pc), was used as a mixture of four structural isomers. The examined Zn(*t*-Bu$_4$Pc) gave fully satisfactory ^{1}H NMR (600 MHz) and MALDI-TOF MS (The synthetic conditions were almost the same with our previous one[15]).

Anhydrous solvents were prepared according to general procedures[37] as follows: Dichloromethane (CH_2Cl_2), pyridine (Py), acetonitrile (MeCN), and benzonitrile (PhCN) were distilled over CaH_2. Tetrahydrofuran (THF) was distilled over sodium/benzophenone ketyl. *N*,*N*-Dimethylformamide (DMF) was distilled over CaH_2 and then over P_2O_5 under reduced pressure, followed

by passing through an alumina column. *N*,*N*-Dimethylacetamide (DMA) was purified by vacuum distillation over CaH_2 and then over CaO.

Coordinating additives were obtained as follows; 1-methylimidazole (MeIm) and pyridine were distilled over CaH_2 under reduced pressure. 3-Acetylpyridine (PyAc), 3-chloropyridine (PyCl), and 3-cyanopyridine (PyCN) were used as received. Quaternary ammonium salts were used as supporting electrolytes after purification by recrystallization; tetra-*n*-butylammonium perchlorate (n-$Bu_4N{\cdot}ClO_4$) from ethanol, and tetra-*n*-butylammonium hexafluorophosphate (n-$Bu_4N{\cdot}PF_6$) from methanol. Each electrolyte was dried under reduced pressure prior to use.

Measurements. To avoid aggregation of Zn(t-Bu_4Pc), electrochemical investigations were carried out typically under relatively dilute concentrations, 0.1 mM Zn(t-Bu_4Pc) with 0.1 M supporting electrolyte. The experimental system was kept under deoxygenated condition by continuous argon flow. A conventional three-electrode system was employed, where working and counter electrodes were inserted into the organic sample compartment and connected to the aqueous sat. KCl compartment of Ag/AgCl (sat. KCl) reference electrode via an agar salt bridge. A platinum pad (diameter 1.6 mm) and a platinum wire were used as a working and an auxiliary electrode, respectively. The voltammograms were recorded on a computer-controlled potentiostat (BAS CV-50W) at 25 °C.

Ferrocene (Fc, purchased from Tokyo Kasei Kogyo Co., Ltd.) was used without purification as the reference reagent. The observed redox values against Ag/AgCl reference electrode (vs. Ag/AgCl (sat. KCl)) was referred to the half-wave potentials for ferrocenium/ferrocene (versus $Fc^{+/0}$), to eliminate the experimental error arising from the liquid junction potentials in each solvent system. In the text, only the oxidation potentials were discussed. We attempted observing the reduction step under the same experimental condition, unfortunately the reduction waves were very faint because of non-Faradaic current, probably due to poor solubility or decreased stability of the anionic species.

UV–vis absorption and emission spectra were recorded on a Shimadzu UV-3100PC spectrophotometer and a Hitachi F-4500 spectrometer, respectively. The sample solution in a 1-cm cell was measured at 25 °C under ordinary atmosphere. Emission spectra were observed for ca. 5.0×10^{-7} M of Zn(t-Bu_4Pc) by excitation at 612 nm under aerobic conditions at 25 °C in each solvent. The fluorescence quantum yield (Φ_F) was determined from integrated emission referred to that of Zn(t-Bu_4Pc), 23%, in toluene.[32]

The spectral change during electrolysis was observed by another experimental set-up, a Shimadzu MultiSpec-1500 as a spectrophotometer and a HOKUTO DENKO HSV-150 as a potentiostat. A platinum mesh (80 mesh) as a working electrode sandwiched by two quartz plates was inserted into sample solution in a 1-cm quartz cell. A Pt plate and Ag wire as a counter and a reference electrode, respectively, were placed in the sample solution. A thin layer of the sample solution was monitored during electrolysis under aerobic condition.

We thank Scientific Research (A) (No. 15205020) from the Ministry of Education, Culture, Sports, Science and Technology (MEXT) of the Japanese Government. We are grateful to Prof. Hajime Karatani (Department of Biomolecular Engineering, Kyoto Institute of Technology) for spectroscopic observation of electrolysis and valuable discussions. We appreciate critical review comments from anonymous reviewers, which improved an earlier draft of this manuscript.

Supporting Information

Solvent variation in cyclic voltammograms (Figure S1), absorption and fluorescence spectra (Figure S2), and correlation of half-wave potential with the DN index (Figure S3) are represented in Supporting Information. This material is available free of charge on the Web at: http://www.csj.jp/journals/bcsj/.

References

1 a) A. B. P. Lever, E. R. Milaeva, G. Speiner, in *Phthalocyanines, Properties and Applications*, ed. by C. C. Leznoff, A. B. P. Lever, VCH Publishers, Inc., **1993**, Vol. 3, Chap. 1. b) M. L'Her, A. Pondaven, in *The Porphyrin Handbook*, ed. by K. M. Kadish, K. M. Smith, R. Guilard, Academic Press, **2003**, Vol. 17, p. 117.

2 a) C. F. van Nostrum, R. J. M. Nolte, *Chem. Commun.* **1996**, 2385. b) N. Kobayashi, *Coord. Chem. Rev.* **2002**, *227*, 129. c) G. de la Torre, P. Vázquez, F. Agulló-López, T. Torres, *Chem. Rev.* **2004**, *104*, 3723. d) G. de la Torre, C. G. Claessens, T. Torres, *Chem. Commun.* **2007**, 2000.

3 R. A. Marcus, N. Sutin, *Biochim. Biophys. Acta* **1985**, *811*, 265.

4 A. B. P. Lever, P. C. Minor, *Inorg. Chem.* **1981**, *20*, 4015.

5 a) A. Giraudeau, F.-R. F. Fan, A. J. Bard, *J. Am. Chem. Soc.* **1980**, *102*, 5137. b) T. Nyokong, Z. Gasyna, M. Stillman, *Inorg. Chem.* **1987**, *26*, 548. c) B. Yu, A. B. P. Lever, T. W. Swaddle, *Inorg. Chem.* **2004**, *43*, 4496.

6 R. H. Campbell, G. A. Heath, G. T. Hefter, R. C. S. McQueen, *J. Chem. Soc., Chem. Commun.* **1983**, 1123.

7 Y. Fu, G. Fu, A. B. P. Lever, *Inorg. Chem.* **1994**, *33*, 1038.

8 A. Gouloumis, S.-G. Liu, Á. Sastre, P. Vázquez, L. Echegoyen, T. Torres, *Chem.—Eur. J.* **2000**, *6*, 3600.

9 K. M. Kadish, L. R. Shiue, R. K. Rhodes, L. A. Bottomley, *Inorg. Chem.* **1981**, *20*, 1274.

10 A. S. Hinman, B. J. Pavelich, *J. Electroanal. Chem.* **1989**, *269*, 53.

11 G. R. Seely, D. Gust, T. A. Moore, A. L. Moore, *J. Phys. Chem.* **1994**, *98*, 10659.

12 M. Nappa, J. S. Valentine, *J. Am. Chem. Soc.* **1978**, *100*, 5075.

13 a) H. Isago, C. C. Leznoff, M. F. Ryan, R. A. Metcalfe, R. Davids, A. B. P. Lever, *Bull. Chem. Soc. Jpn.* **1998**, *71*, 1039. b) N. Kobayashi, T. Fukuda, *J. Am. Chem. Soc.* **2002**, *124*, 8021.

14 K. M. Kadish, E. van Caemelbecke, G. Royal, in *The Porphyrin Handbook*, ed. by K. M. Kadish, K. M. Smith, R. Guilard, Academic Press, **2003**, Vol. 8, p. 1.

15 K. Kameyama, M. Morisue, A. Satake, Y. Kobuke, *Angew. Chem., Int. Ed.* **2005**, *44*, 4763.

16 N. Kobayashi, H. Lam, W. A. Nevin, P. Janda, C. C. Leznoff, A. B. P. Lever, *Inorg. Chem.* **1990**, *29*, 3415.

17 D. E. Richardson, H. Taube, *Inorg. Chem.* **1981**, *20*, 1278.

18 a) B. M. Hoffman, J. A. Ibers, *Acc. Chem. Res.* **1983**, *16*, 15. b) T. J. Marks, *Science* **1985**, *227*, 881.

19 a) D. A. Fernández, J. Awruch, L. E. Dicelio, *Photochem. Photobiol.* **1996**, *63*, 784. b) W. J. Schutte, M. Sluyters-Rehbach, J. H. Sluyters, *J. Phys. Chem.* **1993**, *97*, 6069. c) A. R. Monahan, J. A. Brado, A. F. DeLuca, *J. Phys. Chem.* **1972**, *76*, 1994.

20 a) A. B. P. Lever, J. P. Wilshire, *Can. J. Chem.* **1976**, *54*, 2514. b) A. B. P. Lever, J. P. Wilshire, *Inorg. Chem.* **1978**, *17*, 1145.

21 D. Dubois, G. Moninot, W. Kutner, M. T. Jones, K. M. Kadish, *J. Phys. Chem.* **1992**, *96*, 7137.

22 T. Fukuda, S. Homma, N. Kobayashi, *Chem.—Eur. J.* **2005**, *11*, 5205.

23 a) W. R. Scheidt, W. Dow, *J. Am. Chem. Soc.* **1977**, *99*, 1101. b) W. R. Scheidt, *Acc. Chem. Res.* **1977**, *10*, 339.

24 T. Kobayashi, T. Ashida, N. Uyeda, E. Suito, M. Kakudo, *Bull. Chem. Soc. Jpn.* **1971**, *44*, 2095.

25 R. G. Little, B. M. Hoffman, J. A. Ibers, *Bioinorg. Chem.* **1974**, *3*, 207.

26 a) T. Nyokong, Z. Gasyna, M. J. Stillman, *Inorg. Chem.* **1987**, *26*, 1087. b) T. Rawling, H. Xiao, S.-T. Lee, S. B. Colbran, A. M. McDonagh, *Inorg. Chem.* **2007**, *46*, 2805.

27 a) P. Mu, T. Nakao, M. Handa, K. Kasuga, K. Sogabe, *Bull. Chem. Soc. Jpn.* **1991**, *64*, 3202. b) K. Kasuga, K. Asano, L. Lin, T. Sugimori, M. Handa, K. Abe, T. Kikkawa, T. Fujiwara, *Bull. Chem. Soc. Jpn.* **1997**, *70*, 1859.

28 a) V. Gutmann, in *The Donor–Acceptor Approach to Molecular Interactions*, Plenum Press, New York, **1978**. b) V. Gutmann, *Coord. Chem. Rev.* **1967**, *2*, 239. c) V. Gutmann, *Coord. Chem. Rev.* **1976**, *18*, 225. d) U. Mayer, *Pure Appl. Chem.* **1979**, *51*, 1697. e) P. C. Maria, J. F. Gal, J. de Franceschi, E. Fargin, *J. Am. Chem. Soc.* **1987**, *109*, 483.

29 L. A. Bottomley, K. M. Kadish, *Inorg. Chem.* **1981**, *20*, 1348.

30 C. Alexiou, A. B. P. Lever, *Coord. Chem. Rev.* **2001**, *216–217*, 45.

31 a) P. Suppan, *J. Photochem. Photobiol., A* **1990**, *50*, 293. b) K. Jerwin, F. Wasgestian, *Spectrochim. Acta, Part A* **1984**, *40*, 159. c) H. Isago, Y. Kagaya, A. Matsushita, *Chem. Lett.* **2004**, *33*, 862.

32 T. H. Tran-Thi, C. Desforge, C. Thiec, S. Gaspard, *J. Phys. Chem.* **1989**, *93*, 1226.

33 a) N. Mataga, Y. Kaifu, M. Koizumi, *Bull. Chem. Soc. Jpn.* **1955**, *28*, 690; **1956**, *29*, 373. b) E. Lippert, *Z. Naturforsch.* **1955**, *10a*, 541; E. Lippert, *Z. Elektrochem* **1957**, *61*, 962.

34 M. S. Davis, A. Forman, J. Fajer, *Proc. Natl. Acad. Sci. U.S.A.* **1979**, *76*, 4170.

35 a) H. Konami, M. Hatano, *Chem. Lett.* **1988**, 1359. b) N. Kobayashi, N. Sasaki, Y. Higashi, T. Osa, *Inorg. Chem.* **1995**, *34*, 1636. c) N. Kobayashi, H. Ogata, N. Nonaka, E. A. Luk'yanets, *Chem.—Eur. J.* **2003**, *9*, 5123. d) N. Kobayashi, S. Nakajima, H. Ogata, T. Fukuda, *Chem.—Eur. J.* **2004**, *10*, 6294. e) R. Li, X. Zhang, P. Zhu, D. K. P. Ng, N. Kobayashi, J. Jiang, *Inorg. Chem.* **2006**, *45*, 2327.

36 M. Morisue, Y. Kobuke, *Chem.—Eur. J.* **2008**, *14*, 4993.

37 W. L. F. Armarego, C. L. L. Chai, in *Purification of Laboratory Chemicals*, Fifth Edition Elsevier, **2002**.